Journal of Petroleum Science and Engineering 184 (2020) 106517

Contents lists available at ScienceDirect

Journal of Petroleum Science and Engineering

journal homepage: http://www.elsevier.com/locate/petrol

Experimental investigation into hydraulic fracture geometry and proppant migration characteristics for southeastern Sichuan deep shale reservoirs

Peng Tan [a,1], Huiwen Pang [b,1], Ruxin Zhang [c,*], Yan Jin [b], Yingcao Zhou [a], Jiawei Kao [b], Meng Fan [b]

[a] CNPC Engineering Technology R&D Company Limited, Beijing 102206, China
[b] State Key Laboratory of Petroleum Resources and Prospecting, China University of Petroleum, Beijing 102249, China
[c] Harold Vance Department of Petroleum Engineering, Texas A & M University, College Station, TX 77843-3116, USA

ARTICLE INFO

Keywords:
Hydraulic fracturing
Deep shale
Proppant migration
Bedding plane

ABSTRACT

Difficulties in fracture extension and proppants adding were two key factors that affected the stimulated volume of deep shale reservoir. To clarify the mechanism of hydraulic fracture (HF) propagation and proppants migration, several groups of large-scale true tri-axial fracturing tests with an ingenious method of sand adding were performed utilizing deep Longmaxi shale outcrops from southeastern Sichuan. The interaction behavior between vertical HF and bedding plane (BP) was discussed. The results showed that due to the low bonding strength, the BPs could be easily activated even under high vertical stress difference coefficient. Based on the different influenced degrees of BPs, four types of HF geometries in the vertical direction were observed, that is, transverse HF, horizontal HF, step-shaped HF with fissure opening, and multilateral step-shaped HF network. The migration distance of proppants was limited and almost all the proppants were distributed around the wellbore, thus inducing the formation of multiple secondary HFs. When there are natural fractures (NFs) with large aperture around the wellbore, proppants almost entirely distributed along the NFs. The main factor, causing the difficulty of fracture extension and proppants migration, was the complex HF geometry characterized by the multi-branched fractures with slippage of BPs.

1. Introduction

Deep shale formation, of which the buried depth was more than 3500 m (Chen and Zeng, 2016; Jiang et al., 2017a), had a high economic development value because of rich resource of 4612×10^8 m^3 in Southeast Sichuan, China (Jiang et al., 2017a). Field application indicated that hydraulic fracturing was the key technology to enhance single well production of shale gas. Last decade, the commercial exploitation of shallow shale gas (buried deep was less than 3500 m) was achieved by the combination of two technologies, including horizontal well and staged fracturing. However, lots of challenges and problems appeared in the development for deep shale gas by hydraulic fracturing (Chen and Zeng, 2016; Jiang et al., 2017b).

Geological features of shale gas and the effects of that on hydraulic fracturing had a greatly change due to the increase in buried depth, which mainly included the following aspects. (1) Structural compression effect was strong during post-sedimentary period, resulting in abnormal development of BPs and joints with a weak cementing strength (Fan et al., 2018); (2) A high temperature and high pressure leaded to a high plasticity and difficult fracture extension (Fan et al., 2018; Zeng et al., 2016); (3) An increase in in-situ stress resulted in a high compaction degree and strength of rock matrix (Chen and Zeng, 2016); (4) A high closure pressure caused narrow fracture width and difficulties in proppant migration (Chen and Zeng, 2016). Therefore, two important issues were required to be solved for an effective hydraulic fracturing in deep shale well: how to improve the complex of fracture network during hydraulic fracturing and to enhance fracture conductivity after hydraulic fracturing.

HF morphology and extension range were mainly affected by geological and engineering factors. Field fracturing results indicate that fracture geometry was more complex in shale formation than that in sandstone formation due to the existence of BPs and NFs (Fish et al., 2002; Maxwell et al., 2006). The interaction rule of HF and single NF had been investigated widely. Lamont and Jessen (1963), Zhou et al.

* Corresponding author.
E-mail addresses: tanpeng09jy@163.com (P. Tan), phw9999@126.com (H. Pang), 517956254@qq.com (R. Zhang).
[1] The authors have equal contribution to this work.

https://doi.org/10.1016/j.petrol.2019.106517
Received 4 December 2018; Received in revised form 9 August 2019; Accepted 20 September 2019
Available online 23 September 2019

(2008), and Dehghan et al. (2015) conducted indoor experiments to study the interaction rule of HF and single NF. The results claim that NF occurrence and horizontal stress difference are the two key factors to determine the HF propagation behavior when it encounters the NF. To predict whether HF could cross NF or not, Warpinski and Teufel (1987), Renshaw and Pollard (1995), and Gu and Weng (2010) established the models for the interaction of HF and NF under different suppose conditions. Zhao et al. (2015) and Chuprakov and Prioul (2015) improved above models by considering the change rule of the stresses that were distributed on NF surface. Cheng et al. (2014) and Li et al. (2016) built 3D mathematic models to discuss the interaction behavior between HF and NF.

HF morphology and extension range were mainly affected by geological and engineering factors. Field fracturing results indicate that fracture geometry was more complex in shale formation than that in sandstone formation due to the existence of BPs and NFs (Fish et al., 2002; Maxwell et al., 2006). The interaction rule of HF and single NF had been investigated widely. Lamont and Jessen (1963), Zhou et al. (2008), and Dehghan et al. (2015) conducted indoor experiments to study the interaction rule of HF and single NF. The results claim that NF occurrence and horizontal stress difference are the two key factors to determine the HF propagation behavior when it encounters the NF. To predict whether HF could cross NF or not, Warpinski and Teufel (1987), Renshaw and Pollard (1995), and Gu and Weng (2010) established the models for the interaction of HF and NF under different suppose conditions. Zhao et al. (2015) and Chuprakov and Prioul (2015) improved above models by considering the change rule of the stresses that were distributed on NF surface. Cheng et al. (2014) and Li et al. (2016) built 3D mathematic models to discuss the interaction behavior between HF and NF.

HF morphology and extension range were mainly affected by geological and engineering factors. Field fracturing results indicate that fracture geometry was more complex in shale formation than that in sandstone formation due to the existence of BPs and NFs (Fish et al., 2002; Maxwell et al., 2006). The interaction rule of HF and single NF had been investigated widely. Lamont and Jessen (1963), Zhou et al. (2008), and Dehghan et al. (2015) conducted indoor experiments to study the interaction rule of HF and single NF. The results claim that NF occurrence and horizontal stress difference are the two key factors to determine the HF propagation behavior when it encounters the NF. To predict whether HF could cross NF or not, Warpinski and Teufel (1987), Renshaw and Pollard (1995), and Gu and Weng (2010) established the models for the interaction of HF and NF under different suppose conditions. Zhao et al. (2015) and Chuprakov and Prioul (2015) improved above models by considering the change rule of the stresses that were distributed on NF surface. Cheng et al. (2014) and Li et al. (2016) built 3D mathematic models to discuss the interaction behavior between HF and NF.

HF morphology and extension range were mainly affected by geological and engineering factors. Field fracturing results indicate that fracture geometry was more complex in shale formation than that in sandstone formation due to the existence of BPs and NFs (Fish et al., 2002; Maxwell et al., 2006). The interaction rule of HF and single NF had been investigated widely. Lamont and Jessen (1963), Zhou et al. (2008), and Dehghan et al. (2015) conducted indoor experiments to study the interaction rule of HF and single NF. The results claim that NF occurrence and horizontal stress difference are the two key factors to determine the HF propagation behavior when it encounters the NF. To predict whether HF could cross NF or not, Warpinski and Teufel (1987), Renshaw and Pollard (1995), and Gu and Weng (2010) established the models for the interaction of HF and NF under different suppose conditions. Zhao et al. (2015) and Chuprakov and Prioul (2015) improved above models by considering the change rule of the stresses that were distributed on NF surface. Cheng et al. (2014) and Li et al. (2016) built 3D mathematic models to discuss the interaction behavior between HF and NF.

To clarity HF propagation rule in the fractured formations, numerous investigations in physical experiments and numerical simulation had been conducted. In the respect of experiments, Beugelsdijk et al. (2000) and Zhou et al. (2008) simulated random fracture network in concrete sample by heating treatment and verified the formation of fracture network after hydraulic fracturing. Fan and Zhang (2014) and Liu et al. (2014) summarized that HF initiation and propagation rule in different artificial samples with different NF occurrence. Guo et al. (2014) and Tan et al. (2017, 2018, 2019a) conducted laboratory experiments on shale outcrops to investigate the influences of geological and engineering factors on HF geometry. The fracture network formation capacity of rock is evaluated by a new proposed method (Guo et al., 2015). To monitor the HF propagation path, Chitrala et al. (2013) used AE technology to analysis the features of acoustic responds in different fracturing stages. In the respect of numerical simulation, based on extended finite element method, Fu et al. (2013) considered the stress shadow between the NF and HF and fluid dynamics in a discrete fracture network, simulating HF propagation process in naturally fractured formation. Damjanac and Cundall (2016) utilized discrete element method to simulate the process of HF crossing NF in the three-dimensional space. Kumar and Ghassemi (2016) used displacement discontinuity method to establish fluid-solid coupling model of horizontal well staged fracturing for studying HF propagation. Cohesive zone model that coupled stress-seepage-damage field in Abaqus was utilized to study the fracture propagation behavior (Zhu et al., 2015; Guo et al., 2015a, 2015b; Haddad and Kamy, 2016; Haddad et al., 2017; Li et al., 2017).

Above studies ignored the change in fracture height and only discuss the HF propagation behavior in the horizontal direction. Whereas, for laminated shale formation, BPs have a greatly impact on HF vertical propagation. Complex HF geometry could also be generated in vertical plane (Shan et al., 2018; Zou et al., 2016). According to our previous studies on HF propagation behavior in shallow shale formation, four typical HF morphology types were summarized: simple fracture, fishbone-like fracture, fishbone-like fracture with fissure opening, multilateral fishbone-like fracture network (Tan et al., 2017). Shan et al. (2018) established a modified flow-stress-damage coupling method and investigated the vertical propagation rule of HFs in laminated shales. Zou et al. (2016) studied HF network propagation in naturally fractured layered shale formation based on a 3D discrete element method. Their studies showed that moderate vertical stress anisotropy could not only contain fracture height, but also promote HFs growth in horizontal plane. Ouchi et al. (2017) simulated HF propagation behavior in vertical plane based on peridynamics-based hydrodynamic modeling. Three types of HFs were obtained, including penetration, kinking and bifurcation, which were consistent with the experimental results of AlTammar and Sharma (2017). However, deep shale formation was under the condition of complex tectonic stresses, resulting in high development of BPs and NFs with high angle. Moreover, these discontinuities had a week cementing strength (Fan et al., 2018). Above features for deep shale could cause more complex HF propagation behavior in fracture height direction (Jiang et al., 2017a; Zeng et al., 2016) and mask the rule of proppant migration within induced HFs (Zeng et al., 2016).

To understand the formation mechanism of complex HF network for deep shale, several groups of tri-axial hydraulic fracturing experiments were performed in this paper. Due to the low availability of reservoir cores, fresh outcrops samples were collected from the deep Longmaxi formation located in Chongqing city in the Sichuan basin, southeastern China, as shown in Fig. 1. In addition, an ingenious method of sand adding was proposed to investigate the migration law of proppants within multiple HFs. The research findings would provide a deeper understanding into deep shale fracture geometries and proppants migration affecting by weak BPs and NFs.

2. Geological properties

Southeastern Sichuan locates between Huaying and Qiyue fault

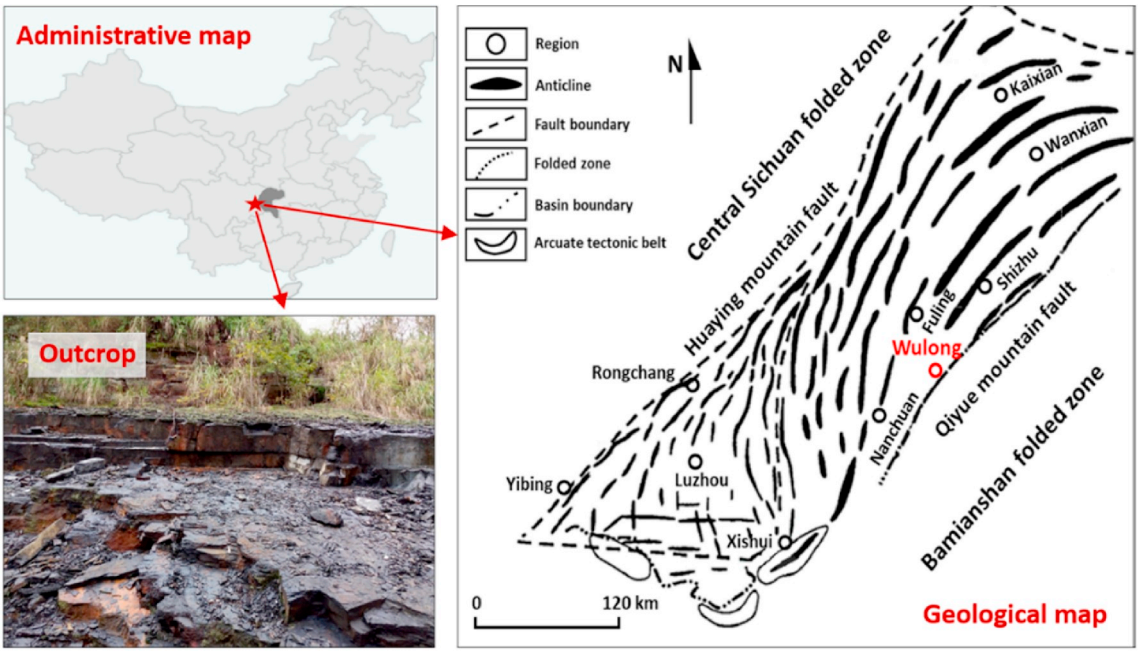

Fig. 1. Location map of the sampling area.

zones (Fig. 1), and Zunyi- Songkan fault zones develops in the south where fold development is the strongest (Chen et al., 2012). In the areas of fold, the closer the edge of the area, the more intense in extrusion deformation of formation (Fan et al., 2018). Deep Longmaxi shale outcrops in this study were collected from Wulong country (Fig. 1) where locates on the boundary of Qiyue fault zone. This area has been affected by severe tectonic compression, so numbers of BPs and high angle NFs are observed on the surface of shale outcrops (Fig. 1). Also, the surfaces of these discontinuities were in a half-filled state or an unfilled state with extremely weak cementing strength (Zeng et al., 2011).

The average porosity of deep Longmaxi shale reservoir in southeastern Sichuan basin tested by well logging was 5.81% (Jiang et al., 2017a). The total organic content and clay (predominately illite) vary from 2.5% to 5.5% and 10.3%–41.3%, respectively. The vitrinite reflectance ranges from 1.85% to 2.23% (Jiang et al., 2017a). The kerogen in the organic matter from the Longmaxi shale formation was predominantly type I and the quality partition of organic content was found to range from and 0.36%–3.31% (average 1.18%) (Chen et al., 2012). The major minerals for Longmaxi shale formation included quartz, calcite, illite and illite-montmorillonite mixture, while feldspar, dolomite, gypsum and pyrite constituted the minor minerals (Chen et al., 2012; Wang et al., 2012). For deep shale, the average proportion of quartz and clay made up of 48.5% and 30%, respectively (Jiang et al., 2017a).

Under the effects of high temperature and high pressure, the plasticity feature of deep shale becomes strong and rock mechanics parameters changed significantly (Zeng et al., 2016). High temperature and high pressure test apparatus (Ge et al., 2010) was used to test mechanic parameters of shale outcrops under different confining pressures and temperatures, as shown in Fig. 2. The results indicated that under low confining pressure and low temperature, elastic deformation was main performance before shale broke; however, in a high confining pressure and high temperature, the plastic stage increased before shale broke and nonlinear deformation characteristics become obvious. Based on brittle evaluation method using energy dissipation (Chen et al., 2017), the energy dissipation was large and rock brittleness decreased greatly under the condition of high temperature and high pressure. As a result, the average brittleness index of samples 4# to 6# was 0.51 times than that of samples 1# to 3#.

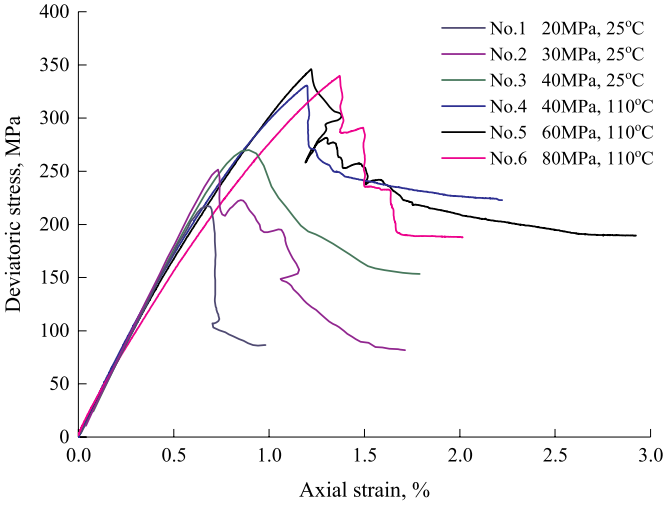

Fig. 2. Stress-strain curves of deep shale under different confining stress and temperature.

The tensile strength of rock matrix and BPs were measured by Brazilian test (Fairhurst, 1964). The results demonstrated that the average tensile strength of rock matrix was 13.17 MPa, whereas, the BP was 1.23 MPa.

3. Experimental method

3.1. Experimental apparatus and sample preparation

Large true tri-axial hydraulic fracturing apparatus was utilized to conduct the experiments on shale samples, as shown in Fig. 3. All samples for experiment were obtained from a large irregular shale outcrop, thereby guaranteeing the similar mechanical properties for all samples. The weathered surfaces of the outcrop were removed, and each final testing block was 30 cm × 30 cm × 30 cm in size (Fig. 4). During the sampling process, the density and placement of BPs in each sample were controlled to a same level as much as possible. The simulated

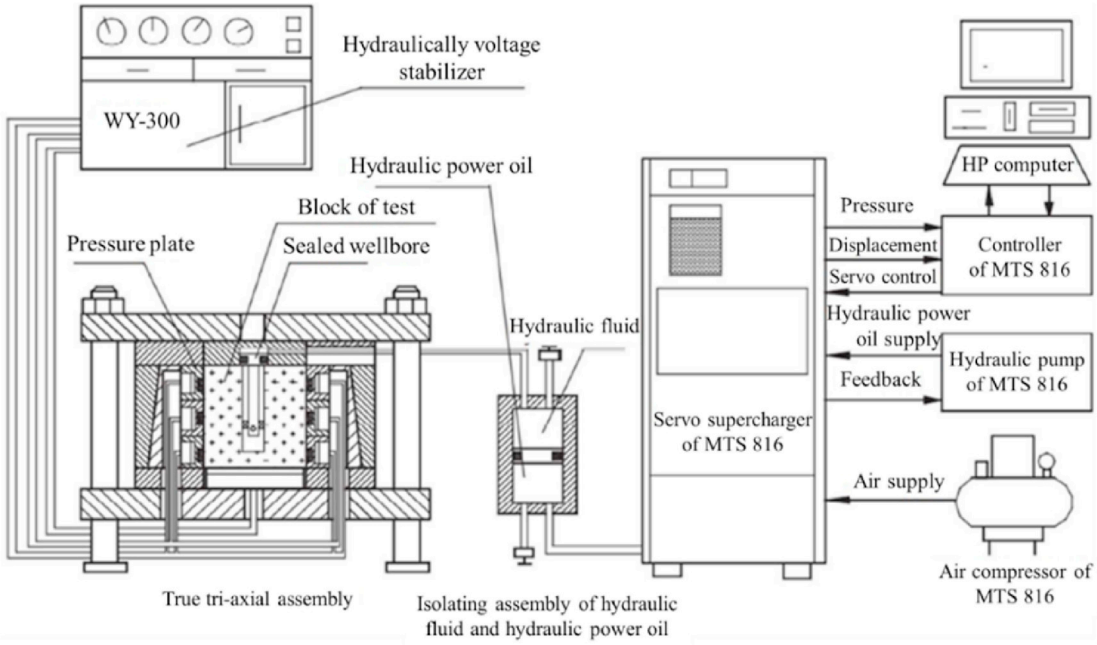

Fig. 3. Schematic of tri-axial experimental equipment (Tan et al., 2017).

wellbore was drilled parallel to the direction of the BP to simulate the horizontal well. The detailed size parameters are shown in Fig. 4(a).

3.2. Experiment procedure

The directions of vertical stress (σ_V), maximum horizontal stress (σ_H), and minimum horizontal stress (σ_h) are applied as shown in Fig. 4 (a) to simulate hydraulic fracturing in the horizontal well. In this work, two different processes of hydraulic fracturing are simulated, including non-sand fracturing and sand fracturing. Non-sand fracturing is the process that single fluid is injected from wellbore into rock that leads to rock broken and HF propagation. Whereas, sand fracturing could be divided into two injection stages, i.e., stage I and stage II. Stage I is the same process as non-sand fracturing. After the complete of stage I, the pump is stopped and then proppants are added into open hole section from the top of the wellbore. In stage II, pump is opened again to inject the sand-carrying fluid to the rock. In this work, the viscosity and injection rate of fluid are same in Stage I and Stage II. Moreover, the amount of proppant (quartz sand with 100 meshes) is 15 g. In each experiment, slick-water with viscosity of 3 mPa s is used as the fracturing fluid, which is widely used in the fracturing treatment of shale formations. Luminous yellow fluorescent dye is added to the fracturing fluid to detect HFs easily. Three types of pump rate, including 12 ml/min, 30 ml/min, and 40 ml/min, are set. Two states of in-situ stress that includes strike-slip fault and normal fault are simulated. The effect of in-situ stress on HF vertical propagation behavior could be attributed to the vertical stress difference coefficient $K_V = (\sigma_V - \sigma_h)/\sigma_h$ (Tan et al., 2017). The detailed experimental parameters are listed in Table 1.

4. Experiment results and analysis

4.1. Experimental results

4.1.1. HF morphology

Several groups of experiments were carried out to investigate HF propagation behavior of deep shale under different in-situ stress and injection conditions. The experimental results were listed in Table 1.

After each experiment, sample was opened along induced fractures to observe HF morphology. Fig. 5 displayed induced HF morphology in each sample. The left side of each picture in Fig. 5 was the reconstitution

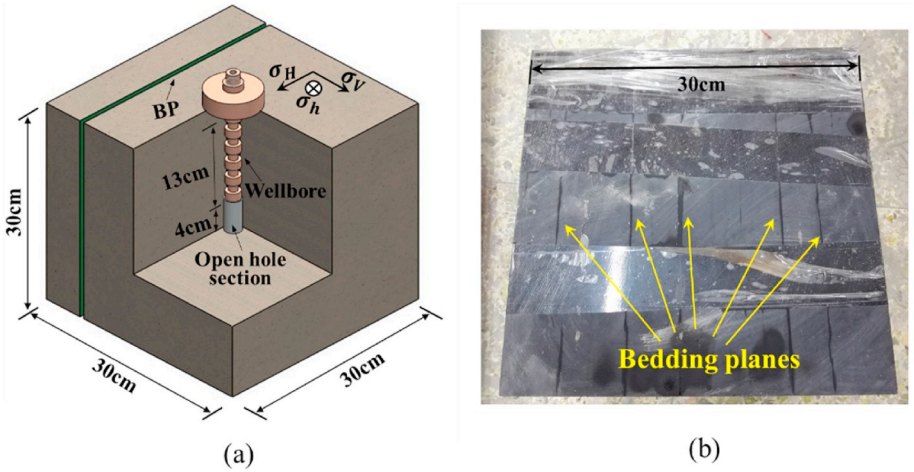

Fig. 4. Illustration of testing block. (a) Schematic diagram; (b) real shale sample.

Table 1
Experimental parameters and results.

Sample	Stress state (MPa)			Vertical stress difference coefficient	Fluid viscosity, mPa·s	Injection rate, ml/min	Sand adding Yes (Y) or Not(N)	Breakdown pressure,MPa	Pressure drop,MPa	Results
	σ_V	σ_H	σ_h	K_V						
1#	22	25	19	0.15	3	40	N	43.32	41.01	Horizontal HF
2#	22	25	16	0.375	3	40	N	50.43	41.58	Horizontal HF
3#	25	20	3	7.3	3	30	N	13.69	9.09	Transverse HF
4#	25	20	13	0.92	3	30	N	18.99	10.59	Transverse HF
5#	25	20	8	2.125	3	30	N	44.45	7.61	Multilateral step-shaped HF network
6#	22	25	20	0.1	3	12	Y	48.2	6.355	Step-shaped HF with fissure opening
7#	22	25	15	0.47	3	12	Y	43.05	42.91	Multilateral step-shaped HF network

sketches, in which blue planes represent BP, red planes represent transverse HF or step-shaped HF, yellow planes represent NF, and green planes represent secondary HF. For interpretation of the references to colour in the figure legend in Fig. 5, the reader is referred to the web version of this article. The results indicated that the magnitude and direction of in-situ stress are not the only factor to determine HF initiation and propagation. Complex HF morphology was generated in deep shale formation due to the influence of BPs and NFs. Similar to previous studies (Guo et al., 2014; Tan et al., 2017; Zhang et al., 2019), three types of HF intersections with a weak plane, namely, penetration, deflection, and termination were observed. Based on the interaction between HFs and discontinuities in the vertical direction, HF morphology could be divided into four categories (Fig. 6):

(1) Horizontal HF. As shown in Fig. 5, Samples 1# and 2# initiated and propagated along a BP, forming single horizontal HF which is horizontal to wellbore and vertical to σ_V. The observation of HF surface claims that this horizontal HF is planar type.

(2) Transverse HF. Samples 3# and 4# initiated and propagated along the direction that is vertical to wellbore, forming single transverse HF which is vertical to BP and σ_h. The transverse HF crossing the BPs indicates that they are also planar type.

(3) Step-shaped HF with fissure opening. Under the effects of BPs which have a weak cementing strength, main HF would deflect into BP to propagate, and then return to the direction perpendicular to the wellbore (sample 5#, 6#), forming step-shaped HF. During the propagation process of main HF, some BPs or NFs nearby were activated, thus forming a non-planar complex HF of step-shaped HF with fissure opening (Fig. 6).

(4) Multilateral step-shaped HF network. Compared with the third HF type, when HF propagated along the BPs, some multiple parallel secondary fractures could be induced at different position in BPs (sample 5#, 7#), thus forming a non-planar and multilateral step-shaped HF network (Fig. 6).

Through our previous experimental studies (Tan et al., 2017), HF takes a shape of fishbone in the vertical direction for shallow shale

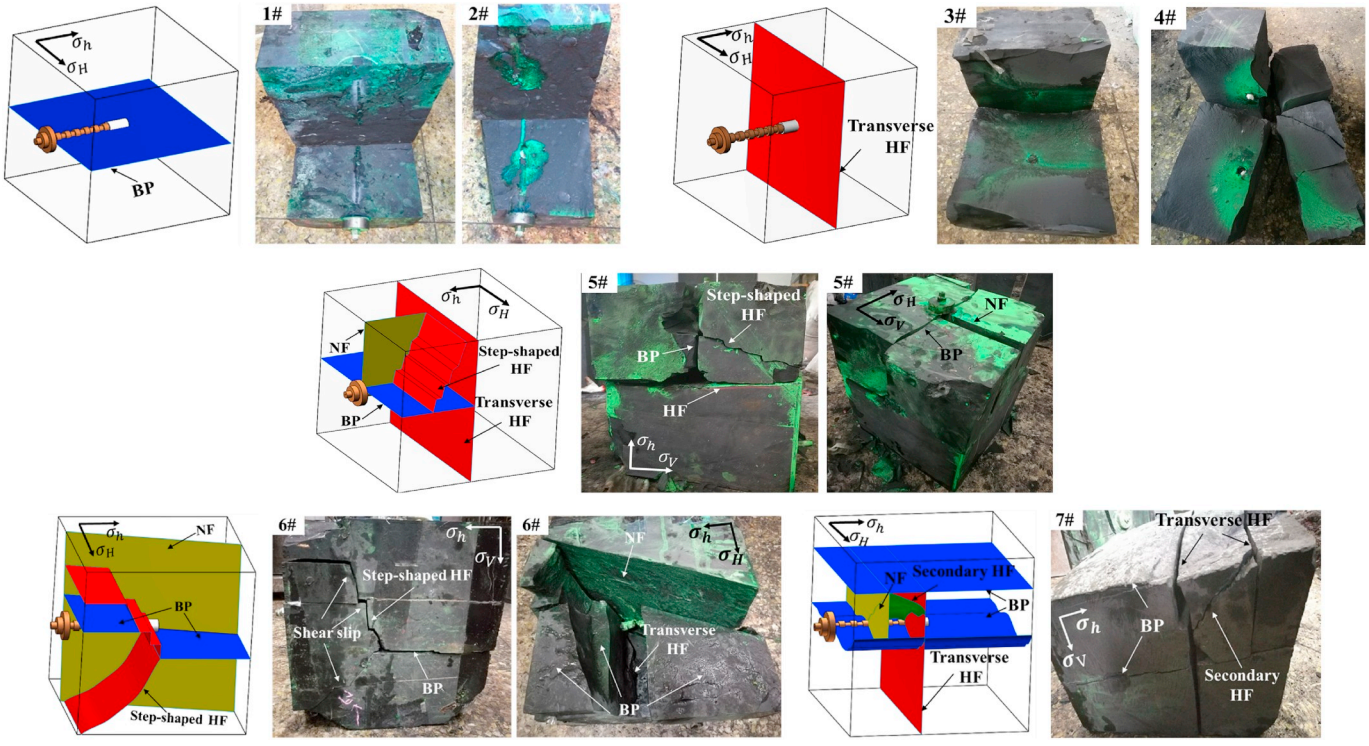

Fig. 5. HF geometries of each sample (blue planes represent BP; red planes represent transverse HF or step-shaped HF; yellow planes represent NF; green planes represent secondary HF). (For interpretation of the references to colour in this figure legend, the reader is referred to the Web version of this article.)

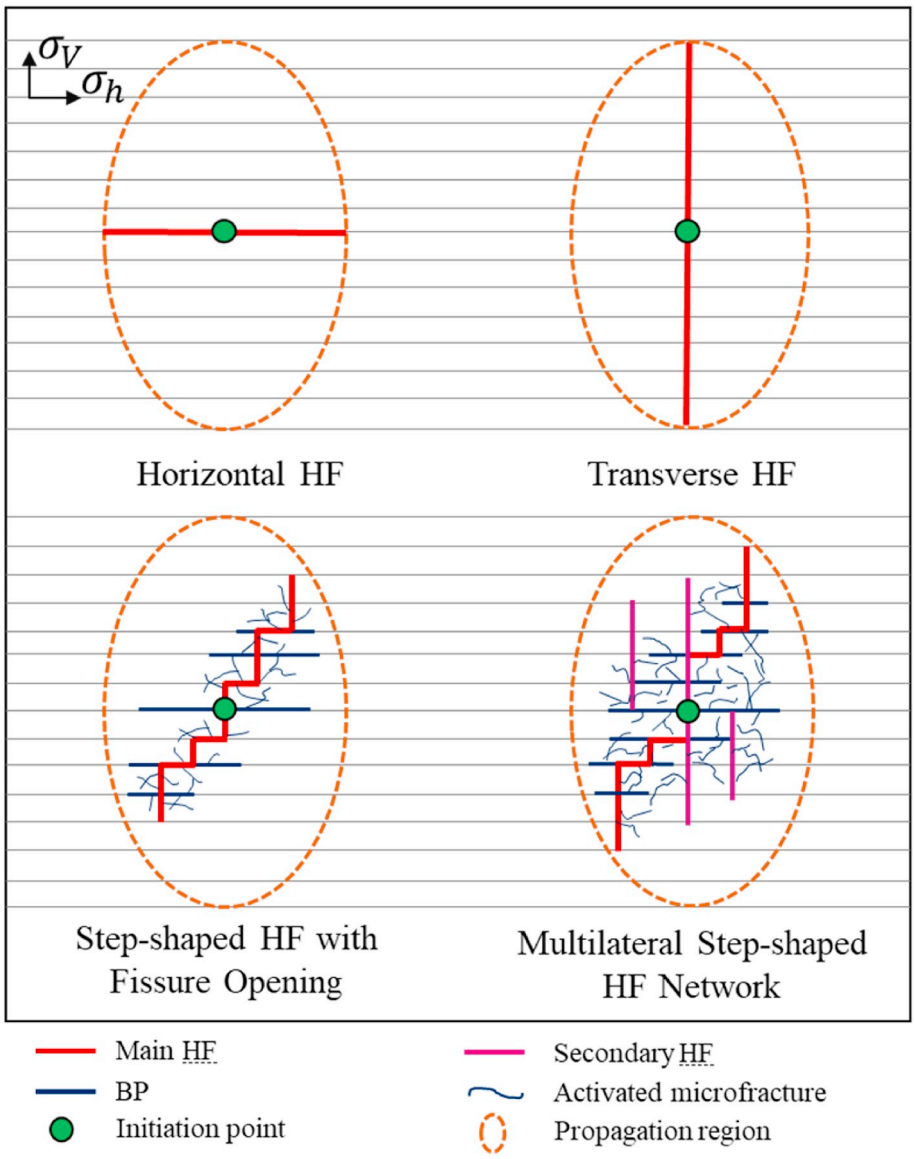

Fig. 6. Schematic diagrams of HF propagation pattern in vertical plane.

formation. Because the effect of tectonic compression in the shallow shale was small, BPs and NFs was in filled state and have a high cementing strength. As a result, HF would firstly cross through the vertical weak structural planes, and then these discontinuities could be activated to some extent due to fluid filtration effects. However, the effect of tectonic compression was intense and the cementing strength of BPs was extremely low in the deep shale. In this paper, the experimental results showed that even under the condition of high vertical stress difference coefficient ($K_V = 2.125$ for sample 5#), HF could deflect to BPs, and forming steps-shape nonplanar fracture. Compared with HF morphology in the shallow shale formation, main HF deflection continuously reduced the fracture width and increased the difficulty of HF propagation in deep shale formation. The results could provide scientific explanation for small fracture height, high fracturing pressure, and limited proppant migration distance in deep shale formation (Jiang et al., 2017a; Zeng et al., 2016; Hu et al., 2018).

4.1.2. *Fracturing pressure response*

The curves of injection pressure versus time for each sample were shown in Fig. 7, which could indirectly reflect the generation of HFs and interactions with weak discontinuities. As fracturing fluid is pumped into the simulated wellbore, injection pressure increases gradually. It drops sharply after reaching a peak point (i.e., the breakdown pressure), which implies that HF initiates from the open hole section of the wellbore. Then, injected fluids drive the HF to extend continuously until the boundary of the sample is reached. Generally, the extension pressure is lower than the breakdown pressure. Previous studies (Wei et al., 2017; Tan et al., 2019b) showed that the fluctuation amplitude of pressure curve was irrelevant to the generation of complex HFs. A slight fluctuation might indicate the opening of new HFs and connection with NFs.

Based on above four typical fracture morphologies, three kinds of pressure responses of HF initiation and propagation could be summarized (Fig. 7): (1) For single horizontal HF initiation and propagation. HF initiation needed to come over the vertical stress, resulting in a high breakdown pressure. When rock began to rupture, high pressure within the wellbore would promote HF to go through the whole BP sharply which had a weak cementing strength fast, thus leading to a high pressure drop. Results showed that the average breakdown pressure and average pressure drop of samples 1# and 2# were 46.88 MPa and 41.3 MPa, respectively. (2) For single transverse HF initiation and propagation. HF initialed and propagated along the direction orthogonal to the minimum horizontal stress, resulting in a low breakdown pressure

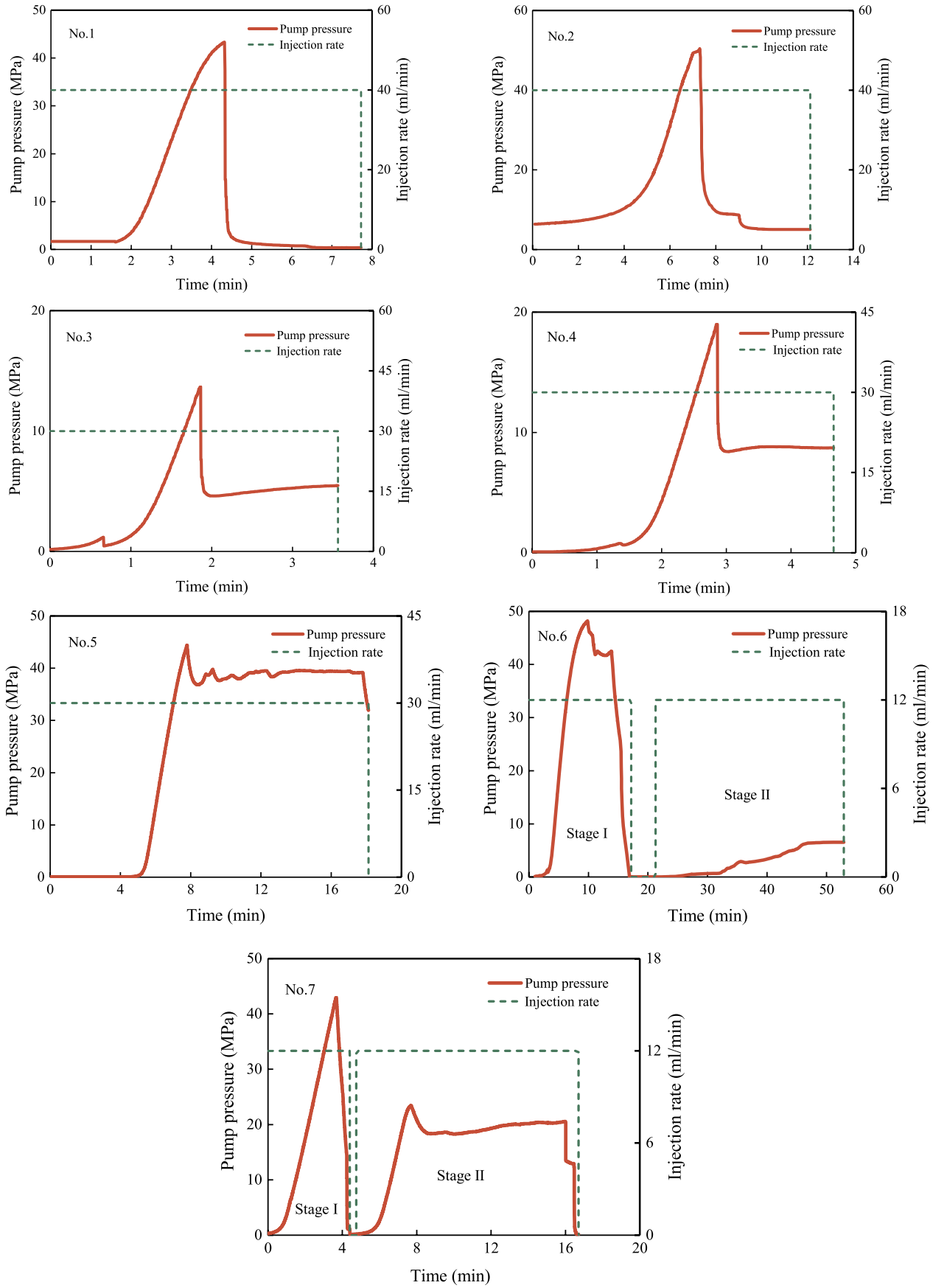

Fig. 7. Injection pressure curves for each sample after hydraulic fracturing.

and pressure drop. Results showed that he average breakdown pressure and average pressure drop of samples 3# and 4# were 16.34 MPa and 9.84 MPa, respectively. (3) For the multiple HFs initiation and propagation. Hydraulic energy was reduced by multiple HFs, increasing friction in the fractures, resulting in a high breakdown pressure and a low pressure drop. Results showed that the breakdown pressure and pressure drop of sample 5# were 44.45 MPa and 7.61 MPa.

According to above analysis results of pressure response characteristics, the type of HF initiation and propagation for sample 6# and 7# could be determined in the non-sand adding process of stage I. The features in sample 6#, a high fracturing pressure (48.2 MPa) and a low pressure drop (6.355 MPa), showed that multiple fractures could initiate simultaneously. As shown in Fig. 5, three HFs (includes one transverse HF, one NF, and one BP) were observed at the open-hole section. According to the pressure analysis, these multiple HFs were induced in the stage I. However, features in sample 7#, a high fracturing pressure (43.05 MPa), a high pressure drop (42.91 MPa) and no stable time for HF propagation in fracturing curve (Fig. 7), demonstrated that HF initiated and propagated along BP. As shown in Fig. 5, some HFs, including one opened BP, one transverse HF, and some secondary HFs, existed at the open-hole section. According to the pressure analysis, the BP was induced in the stage I, whereas, other HFs were generated in the stage II. More detailed analyses on sand fracturing would be conducted in the subsequent subsections.

4.2. Analysis on experimental results

4.2.1. Effect of hydraulic sand fracturing

In this study, hydraulic sand fracturing experiment was carried out for sample 6# and 7# to investigate proppant migration law within fractures and its effects on HF geometries. The results were shown in Figs. 5 and 8.

There is a high angel NF near the wellbore in the sample 6#. In the process of stage II using sand-carrying fluid, fracturing fluid overflowed along the boundary of the sample as the injection pressure increased to 6 MPa slowly. It demonstrated that the fracturing fluid mainly flowed along the multi-fracture channel formed in stage I and there would be no more new HFs in stage II. Besides, under the effect of the NF near the wellbore, proppants would migrate along the NF surface basically and took a shape of ellipse over with the longest distance of 10.3 cm from wellbore, as shown in Fig. 8. In contrast, there was no NF near the wellbore in sample 7#. According to the preceding analysis, it was known that only the BP was opened in stage I. Subsequently, with the injection of sand-carrying fluid in stage II, most of proppants accumulated in the wellbore and plugged the initial open BP, resulting in the increase of pressure in the wellbore again. Fig. 7 showed that when the pressure reached 20.41 MPa in stage II, and the new rupture grows. Based on the analysis of the preceding pressure characteristics, the rupture accords with the characteristics of transverse HF. From the HF morphology after fracturing in Figs. 5 and 8, we could observe the transverse HF clearly near the wellbore. Simultaneously, there were many induced secondary HFs along the direction of BP near the wellbore, which was related to the high extension pressure. The results showed that proppants were mainly distributed on the surface of transverse HF. The shape of proppants distribution was also elliptical, and the longest distance from the open hole section was 5.1 cm, as shown in Fig. 8.

From the above analysis, it could be concluded that proppant migration distance within HFs was pretty limited and most of them were accumulated at the bottom of the wellbore (Fig. 8), which was consistent with the results of microseismic monitoring in field (Jonathan, 2014). Furthermore, HFs activated previously could be plugged by the proppants, which would induce plenty of secondary HFs and made HF morphology more complicated. In addition, the developed NFs with large aperture attracted almost all of the proppants and leaving the main HF with non-propped, which would affect the finial fracturing effect significantly.

4.2.2. Effect of BP and in-situ stress

Based on previous studies (Beugelsdijk et al., 2000; Liu et al., 2014; Tan et al., 2018), in-situ stress and property of BPs played a key role in determining the complexity of HFs in the vertical direction. Many criteria on the interaction between HF and NF with different occurrence were established (Warpinski and Teufel, 1987; Renshaw and Pollard, 1995; Gu and Weng, 2010; Cheng et al., 2014; Li et al., 2016). Considering that the intersection angle between HF and BPs was orthotropic, the criterion between HF and orthotropic NF proposed by Renshaw and Pollard (1995) was selected in this paper to study the effect of vertical stress difference coefficient and friction coefficient of BP on HF vertical propagation. Based on the mechanical criterion (Renshaw and Pollard,

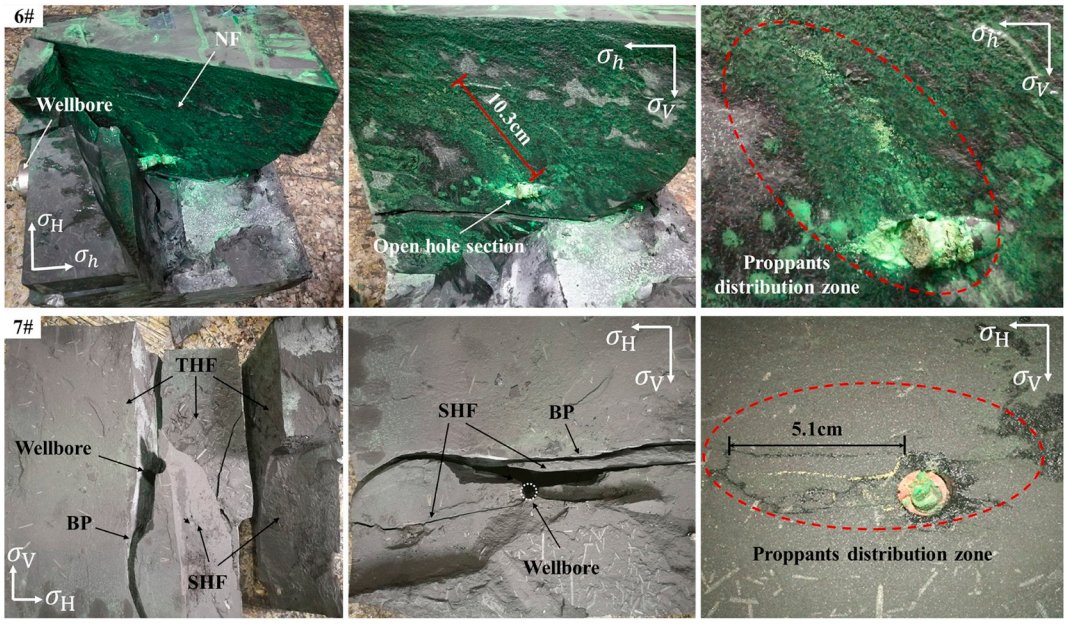

Fig. 8. HF geometries of sample 6# and 7#.

1995), the critical condition for the vertical penetration of a HF through the BP was (prescribed compressive stress was positive and tensile stress was negative):

$$\frac{\sigma_v}{\sigma_h - T_0} = \frac{0.35 + \frac{0.35}{\mu_0}}{1.06} \quad (1)$$

In which, σ_V is vertical stress, MPa; σ_h is minimum horizontal stress, MPa; T_0 is tensile strength of shale matrix; μ_0 is the critical value of friction coefficient of BP. Through the experimental parameters of in-situ stress in this study, the friction coefficient (μ_0) of BP could be calculated. The calculation results were shown in Table 2.

The relationship between critical friction coefficient of BP and vertical stress difference coefficient was shown in Fig. 9. Results showed that there was a negative correlation between friction coefficient of BP and vertical stress difference coefficient. The smaller the difference of vertical stress was, the higher the critical friction coefficient of BP was required for penetrating the BP. Affecting by tectonic movement in the post-sedimentary period, deep shale formation was in the state of strike-slip stress or reverse fault stress (Shan et al., 2015), and BPs or NFs were almost in the state of half-filling or even non-filling (Zeng et al., 2011). As a result, both the vertical stress difference coefficient and friction coefficient of BPs were too small. Therefore, for hydraulic fracturing of deep shale formation, deflection and propagation along the BPs could easily occur, contributing to the formation of multilateral step-shaped HF network fracture in the vertical plane.

4.3. *Patterns of complex HF network*

From the experimental observations and analyses described above, three patterns of HF network in vertical plane were summed up according to the lateral distribution of HF in vertical profile, as shown in Fig. 10.

Pattern A: HF network with small horizontal sweep region. For this pattern of HF network, the main HF was characterized by straightness, large length, and wide width, and meanwhile little discontinuities were activated and thus decreasing the number of secondary HFs. To form a HF network like this pattern, the super-deep shale formation with large vertical stress difference coefficient or shallow shale formation without tectonic compression was expected.

Pattern B: HF network with medium horizontal sweep region. For this pattern of HF network, the main HF was characterized by straightness, moderate length, and medium width, and meanwhile some secondary HFs were activated. To form a HF network like this pattern, shallow shale formation with little tectonic compression was expected. The fracture morphology of fishbone-like fracture with fissure opening in shallow shale formation in our previous study (Tan et al., 2017) was belong to this fracture pattern.

Pattern C: HF network with large horizontal sweep region. For this pattern of HF network, the main HF was characterized by kink, short length, and narrow width, and meanwhile abundant secondary HFs were activated. To form a HF network like this pattern, deep shale formation with small vertical stress difference coefficient and weak cementing strength of BP was expected. The fracture morphology of step-shaped HF with fissure opening in deep shale formation in this work was belong to this fracture pattern.

Table 2
Experimental and calculative data.

Sample	σ_V(MPa)	σ_h(MPa)	K_V(MPa)	T_0(MPa)	μ_0
1#	22	19	0.15	13.17	0.93
2#	22	16	0.375	13.17	0.78
3#	25	3	7.3	13.17	0.27
4#	25	13	0.92	13.17	0.53
5#	25	8	2.125	13.17	0.39
6#	22	20	0.1	13.17	0.99
7#	22	15	0.47	13.17	0.73

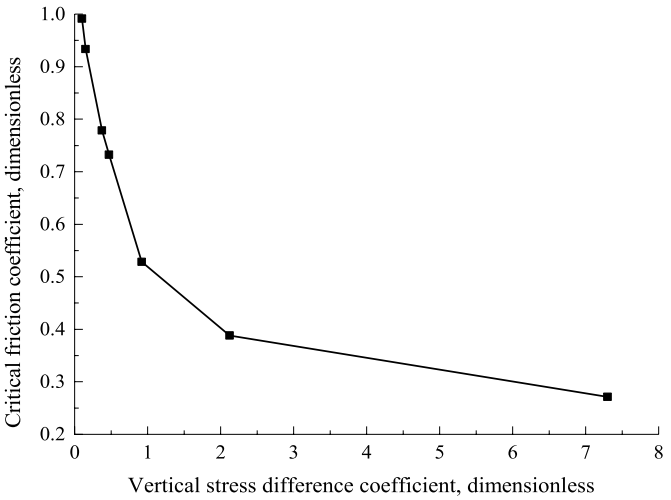

Fig. 9. Relationship between critical friction coefficient and vertical stress difference coefficient.

5. Significance and applicability of results

Four typical fracture types of fracture vertical propagation in deep shale were summarized based on laboratory experiments with small size sample, including horizontal HF, transverse fracture, step-shaped HF with fissure opening, and multilateral step-shaped HF network. When the size was amplified to the infinite formation, the vertical HF morphology of multilateral step-shaped HF network was predominant. The complex HF morphology combining with high closure stress for deep shale, would lead to the increase of HF tortuous degree and the decrease of HF width, which seriously restricting the proppants migration within HFs. To prevent tip screen out during hydraulic fracturing, the main HF morphology, especially the complexity degree of HFs near the wellbore, required to be simplified. Some methods could achieve the goal. For one thing, by optimizing the operation parameters, high fluid viscosity was selected in the initial fracturing stage to increase the chances of HF penetrating weak discontinuities and reduce the generation of secondary HFs near the wellbore. For another thing, a small amount of acid could be injected into formation to improve main HF width near the wellbore by acid reaction (Lu et al., 2018; Guo et al., 2017).

Affecting by intense tectonic movement in the post-sedimentary period, the developed BPs possess weak cementing strength, which could easily induce HFs to deflect or bifurcate along the BPs. Results showed that HF geometry in deep shale formation had a greatly difference with that in shallow shale formation. Fishbone-like HF networks with straight main HF was the main HF morphology in shallow shale formation (Tan et al., 2017), whereas, step-shaped HF network with kinked main HF was the main HF morphology in deep shale formation. The deflection and bifurcation of main fracture for deep shale increased horizontal sweep region, resulting in a short propagation distance of HF height in the vertical plane. Therefore, if traditional two-dimensional fracture height model (such as PKN and KGD) was used for deep shale horizontal well staged fracturing design, the results would have large limitations.

In field operation process, the fracturing curve was one of the important references for engineers to determine the construction status. Proper analysis and explanation of the curves helped understand some phenomenon that could not be observed directly in fracturing process. In this work, three types of pump pressure response characteristics for HF initiation and propagation were analyzed, including single horizontal HF, single transverse HF, and multiple HFs. The conclusions could

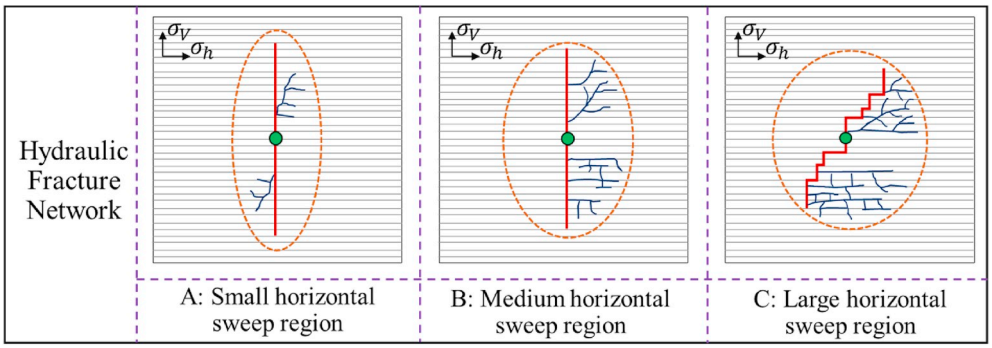

Fig. 10. Pattern of complex HF network.

provide an auxiliary method for real-time controlling of HF propagation, adjusting the operation plan for sudden accidents timely, and reducing the risk of fracturing construction.

Above experimental results showed that sand fracturing had significantly impacts on HF morphology in deep shale formation. Proppants could accumulate easily near the wellbore, inducing the generation of numerous secondary HFs and resulting in premature screen-out easily. Therefore, method of sand adding gradually was recommended in field. Firstly, small size of proppants was used to grind perforation and main HF to reduce the resistance of proppant migration. Then, large size proppants were utilized. In addition, multiple sand adding (Yu et al., 2017) or channel fracturing (Hou et al., 2016) could also improve the distance of proppant migration and fracture conductivity. It was noteworthy that the development of NFs near the wellbore could change the HF morphology and proppant migration path. Thus, to improve the effect of fracturing, it was necessary to avoid conducting fracturing operation in development zones of NFs.

6. Discussion

By conducting the mechanical parameter experiments, it could be found that strength and plastic characteristics of shale increased notably under the effects of high temperature and high pressure (Fig. 2). However, restricted by the limitation of the technique and material for pressure and heating treatment, it was impossible presently to conduct large size true tri-axial fracturing experiment under high temperature and high pressure to completely simulate the true condition in deep shale reservoir. In this study, we could only simulate the coefficient of stress difference instead of the in-situ stresses in the actual formations. Therefore, it was more difficult for HF propagation and proppant migration during the actual process of fracturing operation in deep shale formation. Meanwhile, proppants would embed into rock after fracturing, resulting in more narrow fracture width and more low fracture conductivity. Although new sights and significant results had been achieved in this paper, the results were not entirely representative and could not be extrapolated quantitatively to cannot be used directly in field operation in the field. However, the qualitative law obtained experimentally could provide important basis for understanding HF propagation behavior and optimizing fracturing design in deep shale formation.

The injection rate in this paper referenced to the references (Zhou et al., 2008; Guo et al., 2014; Tan et al., 2017). Up to now, many scholars have made great efforts on transforming injection parameters in laboratory to that in fields. Different similarity criteria (De Pater et al., 1994; Bunger et al., 2005) are set. However, these criteria are all based on the hypotheses of isotropic linear elastomer and elliptical fracture planes. Therefore, these hypotheses cannot be applied to heterogenous and discontinuous shale formations. On the other hand, multi-cluster staged fracturing is often used in cased hole plugs and perforation horizontal wells in shale formation. Limited by the scale of indoor experiments, operations such as casing cementing and helix distribution perforation are difficult to simulate in indoor experiments. In present laboratory studies, helix distribution perforation is neglected and open hole completion is simplified. Hence, it is of great difficulties to quantificationally determine the relation between indoor and field parameters. Further study on similarity criterion in shale plays is required.

In our previous studies (Tan et al., 2017), we have detailedly analyzed the effects of fluid viscosity and injection rate on fracture initiation and propagation geometries. The results show that high injection rate and fluid viscosity are helpful for the penetration of weak planes and thus forming a simple fracture geometry at local, however, the properties of developed weak planes and in-situ stress are the most important factors that dominate hydraulic fracture geometries. For southeastern Sichuan deep shale, the cementing strength of beddings is extremely low, resulting in that these beddings could be easily activated even under the condition of high injection rates and forming the step-shaped fracture geometry. Therefore, the proppants have difficulties in transporting over a long distance within fractures. The injection rate as well as fluid viscosity do have important influences on the local proppant transport and fracture geometries to a certain extent, the finial fracture geometries and proppant transport law were dominated by the properties of weak planes and shale matrix and stress conditions. This paper obtains the similar results with the microseismic monitoring results in field (Jonathan, 2014) that proppant migration distance was pretty limited and most of them were accumulated at the bottom of the wellbore.

Two methods, acoustic emission location (Lu et al., 2018) and high-energy computed tomography (CT) (Patel et al., 2017), were utilized to monitor HF initiation and propagation complementally. However, both failed to obtain the desired results. This might be mainly related to the physical and mechanical properties of deep shale. Due to the poor cementing of developed BPs and NFs in deep shale outcrops, acoustic emission signals prone to decay or deflection when they encounter the discontinuities during the process of hydraulic fracturing, resulting in the loss of signal points or incorrect location. Thus, the locating effect in deep shale could achieve as the same of that in homogeneous sandstone (Patel et al., 2017; He et al., 2017).

In addition, due to the high strength and high density of deep shale matrix, it was of great difficulty for X ray to penetrate into the cube sample of 30 cm on a side, even the accelerator industrial CT equipment with 6 MeV in energy was utilized. Thus, it was necessary to improve the acoustic emission location methods in the future for precise localization of HF propagation in fractured formation. In the meantime, higher energy CT equipment was required to complete the detection and imaging of internal structure for compact rocks.

7. Conclusion

Several groups of large-scale true tri-axial fracturing experiments were conducted to investigate the characteristics of HF propagation and

proppant migration in deep shale formation. Main conclusions of this work could be summarized as follows:

(1) Undergoing severe tectonic movements, deep shale formations were characterized by extremely weak BPs and NFs with high angle. HFs could divert easily and propagate along these discontinuities even under high vertical stress difference coefficient. From experimental observation, HF geometries of deep shale in the vertical plane could be classified into four categories: transverse HF, horizontal HF, step-shaped HF with fissure opening, and multilateral step-shaped HF network.
(2) Different HF initiation and propagation geometries displayed different pressure responses. For a single horizontal HF, both the breakdown pressure and the pressure drop were high; For a single transverse HF, both the breakdown pressure and the pressure drop were small; For multiple HFs, the breakdown pressure was high while the pressure drop was small. The qualitative conclusions could be served as an auxiliary reference during fracturing treatment.
(3) Results showed that hydraulic sand fracturing was a complex process. Most of proppants were easily stacked around the wellbore, while only a fraction of them migrated to a limited range that took a shape of ellipse. The HFs formed in stage I could be sealed by the injected proppants and secondary HFs were induced near the wellbore, which leaded to the formation of multiple secondary HFs. In addition, developed large-aperture NFs near the wellbore could be worked as the path of proppants migration, thus resulting in the closure of main HFs for lack of propping.
(4) Considering the combined effects of in-situ stress and BP properties, three patterns of HF network were proposed based on the size of horizontal sweep region in the vertical plane, namely, HF network with small, medium, and large region. For deep shale formations, the HFs possessed the large horizontal sweep region and short height.

Acknowledgements

The authors gratefully appreciate the support of National Science and Technology Major Projects of China (Grant No. 2016ZX05066).

Appendix A. Supplementary data

Supplementary data to this article can be found online at https://doi.org/10.1016/j.petrol.2019.106517.

References

AlTammar, M.J., Sharma, M.M., 2017. Effect of geological layer properties on hydraulic fracture initiation and propagation: an experimental study. In: SPE 184871 Presented at the SPE Hydraulic Fracturing Technology Conference, Woodlands, Texas.
Beugelsdijk, L.J.L., De Pater, C.J., Sato, K., 2000. Experimental hydraulic fracture propagation in a multi-fractured medium. In: SPE 59419 Presented at the Asia Pacific Conference on Integrated Modelling for Asset Management, Yokohama, Japan.
Bunger, A.P., Jeffrey, R.G., Detournay, E., 2005. Application of scaling laws to laboratory-scale hydraulic fractures. In: ARMA 05 presented at the 40th U.S. Symposium on Rock Mechanics (USRMS). Anchorage, Alaska.
Chen, Z., Zeng, Y.J., 2016. Present situations and prospects of multi-stage fracturing technology for deep shale gas development. Pet. Drilling Tech. 44 (1), 6–11.
Chen, S.B., Zhu, M.Y., Wang, H.Y., et al., 2012. Structure characteristics and accumulation significance of nanopores in Longmaxi shale gas reservoir in the southern Sichuan basin. J. China Coal Soc. 37 (3), 438–444.
Chen, Y., Jin, Y., Chen, M., et al., 2017. Quantitative evaluation of rock brittleness based on the energy dissipation principle, an application to type II mode crack. J. Nat. Gas Sci. Eng. 45, 527–536.
Cheng, W., Jin, Y., Chen, M., et al., 2014. A criterion for identifying hydraulic fractures crossing natural fractures in 3D space. Pet. Explor. Dev. 41 (3), 371–376.
Chitrala, Y., Moreno, C., Sondergeld, C., et al., 2013. An experimental investigation into hydraulic fracture propagation under different applied stresses in tight sands using acoustic emissions. J. Pet. Sci. Eng. 108, 151–161.
Chuprakov, D.A., Prioul, R., 2015. Hydraulic Fracture Height Containment by Weak Horizontal interfaces[C]//SPE 173337 Presented at the Hydraulic Fracturing Technology Conference. Woodlands, Texas.
Damjanac, B., Cundall, P., 2016. Application of distinct element methods to simulation of hydraulic fracturing in naturally fractured reservoirs. Comput. Geotech. 71, 283–294.
De Pater, C.J., Weijers, L., Savic, M., et al., 1994. Experimental study of nonlinear effects in hydraulic fracture propagation. SPE Prod. Facil. (11), 239–248.
Dehghan, A.N., Goshtasbi, K., Ahangari, K., et al., 2015. The effect of natural fracture dip and strike on hydraulic fracture propagation. Int. J. Rock Mech. Min. Sci. 75, 210–215.
Fairhurst, C., 1964. On the validity of the 'Brazilian' test for brittle materials. Int. J. Rock Mech. Min. Sci. Geomech. Abstr. 1, 535–546.
Fan, T.G., Zhang, G.Q., 2014. Laboratory investigation of hydraulic fracture networks in formations with continuous orthogonal fractures. Energy 74, 164–173.
Fan, C.H., Li, H., Zhong, C., et al., 2018. Tectonic fracture stages and evolution model of Longmaxi Formation shale, Dingshan structure, Southeast Sichuan. Acta Pet. Sin. 39 (04), 379–390.
Fish, M.K., Wright, C.A., Davidson, B.M., et al., 2002. Integrating Fracture Mapping Technologies to Optimize Stimulations in the Barnett Shale [C]//SPE 77441 Presented at the Annual Technical Conference and Exhibition. San Antonio, Texas.
Fu, P., Johnson, S.M., Carrigan, C.R., 2013. An explicitly coupled hydro-geomechanical model for simulating hydraulic fracturing in arbitrary discrete fracture networks. Int. J. Numer. Anal. Methods Geomech. 37 (14), 2278–2300.
Ge, W.F., Chen, M., Jin, Y., 2010. Analysis of the external pressure on casings induced by salt- gypsum creep in build-up sections for horizontal wells. Rock Mech. Rock Eng. 44, 711–723.
Gu, H., Weng, X., 2010. Criterion for Fractures Crossing Frictional Interfaces at Non-orthogonal angles[C]//ARMA 198 Presented at the 44th US Rock Mechanics Symposium and 5th US-Canada Rock Mechanics Symposium. Salk Lake City, UT.
Guo, T.K., Zhang, S.C., Qu, Z., et al., 2014. Experimental study of hydraulic fracturing for shale by stimulated reservoir volume. Fuel 128, 373–380.
Guo, T.K., Zhang, S.C., Ge, H.K., et al., 2015. A new method for evaluation of fracture network formation capacity of rock. Fuel 140, 778–787.
Guo, J.C., Zhao, X., Zhu, H.Y., et al., 2015. Numerical simulation of interaction of hydraulic fracture and natural fracture based on the cohesive zone finite element method. J. Nat. Gas Sci. Eng. 25, 180–188.
Guo, J.C., Lu, Q.L., Zhu, H.Y., et al., 2015. Perforating cluster space optimization method of horizontal well multi-stage fracturing in extremely thick unconventional gas reservoir. J. Nat. Gas Sci. Eng. 26, 1648–1662.
Guo, T.K., Li, Y.C., Ding, Y., et al., 2017. Evaluation of acid fracturing treatments in shale formation. Energy Fuels 31 (10), 10479–10489.
Haddad, M., Kamy, S., 2016. XFEM-based CZM for the simulation of 3D multiple-cluster hydraulic fracturing in Quasi-brittle shale formations. Rock Mech. Rock Eng. 49, 4731–4748.
Haddad, M., Du, J., Vidal-Gilbert, S., 2017. Integration of dynamic microseismic data with a true 3D modeling of hydraulic-fracture propagation in the Vaca Muerta shale. SPE J. 1714–1738.
He, J.M., Lin, C., Li, X., et al., 2017. Initiation, propagation, closure, and morphology of hydraulic fractures in sandstone cores. Fuel 208, 65–70.
Hou, B., Zheng, X.G., Chen, M., 2016. Parameter simulation and optimization in channel fracturing. J. Nat. Gas Sci. Eng. 35, 122–130.
Hu, X.D., Wu, K., Li, G.S., et al., 2018. Effect of proppant addition schedule on the proppant distribution in a straight fracture for slickwater treatment. J. Pet. Sci. Eng. 167, 110–119.
Jiang, T.X., Zhou, J., Zhang, X., et al., 2017. Overview and prospect of fracture propagation and conductivity characteristics in deep shale gas wells. Sci. Sin. Phys. Mech. Astron. 47 (11), 114603.
Jiang, T.X., Bian, X.B., Wang, H.T., et al., 2017. Volume fracturing of deep shale gas horizontal wells. Nat. Gas. Ind. 37 (1), 90–96.
Jonathan, P., 2014. Where Did the Proppant Go? [C]//SPE 1922843 Presented at the Unconventional Resources Technology Conference. Denver, Colorado.
Kumar, D., Ghassemi, A., 2016. 3D Poroelastic simulation and analysis of multiple fracture propagation and refracturing of closely-spaced horizontal wells. In: ARMA 136 Presented at 50th US Rock Mechanics/Geomechanics Symposium, Houston, Texas.
Lamont, N., Jessen, F.W., 1963. The effects of existing fractures in rocks on the extension of hydraulic fractures. J. Pet. Technol. 15 (02), 203–209.
Li, Y., Deng, J., Liu, W., et al., 2017. Modeling hydraulic fracture propagation using cohesive zone model equipped with frictional contact capability. Comput. Geotech. 91, 58–70.
Li, S.B., Li, X., Zhang, D.X., et al., 2016. A fully coupled thermo-hydro-mechanical, three-dimensional model for hydraulic stimulation treatments. J. Nat. Gas Sci. Eng. 34, 64–84.
Liu, Z.Y., Chen, M., Zhang, G.Q., 2014. Analysis of the influence of a natural fracture network on hydraulic fracture propagation in carbonate formations. Rock Mech. Rock Eng. 47 (2), 575–587.
Lu, Q., Lu, G., Prioul, R., et al., 2018. Impact of fluid acidity on the time-dependent initiation of hydraulic fractures in carbonate rocks. Rock Mech. Rock Eng. 12 (51), 3895–3906.
Maxwell, S.C., Waltman, C.K., Warpinski, N.R., et al., 2006. Imaging Seismic Deformation Induced by Hydraulic Fracture Complexity [C]//SPE 102801 Presented at the Annual Technical Conference and Exhibition. San Antonio, Texas.
Ouchi, H., Foster, J.T., Sharma, M.M., 2017. Effect of reservoir heterogeneity on the vertical migration of hydraulic fractures. J. Pet. Sci. Eng. 151, 384–408.

Patel, S.M., Sondergeld, C.H., Rai, C.S., 2017. Laboratory studies of hydraulic fracturing by cyclic injection. Int. J. Rock Mech. Min. Sci. 95, 8–15.
Renshaw, C.E., Pollard, D.D., 1995. An experimentally verified criterion for propagation across unbounded frictional interfaces in brittle, linear elastic materials. Int. J. Rock Mech. Min. Sci. Geomech. Abstr. Pergamon 32 (3), 237–249.
Shan, Q.L., Jin, Y., Chen, M., et al., 2015. Causes of and responses to abnormal fracture pressure on ultra-deep shale in Southern China. In: SPE 176951 Presented at the SPE Asia Pacific Unconventional Resources Conference and Exhibition, Brisbane, Australia.
Shan, Q.L., Jin, Y., Tan, P., et al., 2018. Experimental and numerical investigations on the vertical propagation of hydraulic fractures in laminated shales. J. Geophys. Eng. 14pp, 1729–1742.
Tan, P., Jin, Y., Han, K., et al., 2017. Analysis of hydraulic fracture initiation and vertical propagation behavior in laminated shale formation. Fuel 206, 482–493.
Tan, P., Jin, Y., Hou, B., 2018. Laboratory investigation of shale rock to identify fracture propagation in vertical direction to bedding. J. Geophys. Eng. 15, 696–706.
Tan, P., Jin, Y., Hou, B., et al., 2019. Experimental investigation of hydraulic fracturing for multi-type unconventional gas Co-exploitation in Ordos basin. Arabian J. Sci. Eng. https://doi.org/10.1007/s13369-019-03974-9.
Tan, P., Jin, Y., Yuan, L., et al., 2019. Understanding hydraulic fracture propagation behavior in tight sandstone–coal interbedded formations: an experimental investigation. Pet. Sci. 16 (1), 148–160.
Wang, Y.M., Dong, D.Z., Li, J.Z., et al., 2012. Reservoir characteristics of shale gas in Longmaxi formation of the Lower Silurian, southern Sichuan. Acta Pet. Sin. 33 (4), 551–561.
Warpinski, N.R., Teufel, L.W., 1987. Influence of geologic discontinuities on hydraulic fracture propagation. J. Pet. Technol. 39 (02), 209–220.
Wei, D., Gao, Z.Q., Fan, T.L., 2017. Experimental hydraulic fracture propagation on naturally tight intra-platform shoal carbonate. J. Pet. Sci. Eng. 157, 980–989.
Yu, P., Zhong, B.C., Qiao, H.T., et al., 2017. Multi-sanding fracturing technology used for CBM wells. Oil Drill. Prod. Technol. 39 (3), 356–361.
Zeng, X.L., Liu, S.G., Huang, W.M., et al., 2011. Comparison of silurian Longmaxi formation shale of Sichuan basin in China and carboniferous barnett formation shale of fort worth basin United States. Geol. Bull. China 30 (2/3), 372–384.
Zeng, Y.J., Chen, Z., Bian, X.B., 2016. Breakthrough in staged fracturing technology for deep shale gas reservoirs in SE Sichuan basin and its implications. Nat. Gas. Ind. 36 (1), 61–67.
Zhang, R.X., Hou, B., Han, H.F., 2019. Experimental investigation on fracture morphology in laminated shale formation by hydraulic fracturing. J. Petro. Sci. Eng. 177, 442–451.
Zhao, J., Peng, Y., Li, Y., et al., 2015. Analytical model for simulating and analyzing the influence of interfacial slip on fracture height propagation in shale gas layers. Environ. Earth Sci. 73 (10), 5867–5875.
Zhou, J., Chen, M., Jin, Y., et al., 2008. Analysis of fracture propagation behavior and fracture geometry using a tri-axial fracturing system in naturally fractured reservoirs. Int. J. Rock Mech. Min. Sci. Geomech. 45, 1143–1152.
Zhu, H.Y., Zhao, X., Guo, J.C., et al., 2015. Coupled flow-stress-damage simulation of deviated-wellbore fracturing in hard-rock. J. Nat. Gas Sci. Eng. 26, 711–724.
Zou, Y.S., Ma, X.F., Zhang, S.C., et al., 2016. Numerical investigation into the influence of bedding plane on hydraulic fracture network propagation in shale formations. Rock Mech. Rock Eng. 49, 3597–3614.